

Band structure and electro-optical properties of mixed type-I/type-II $\text{In}_x\text{Ga}_{1-x}\text{As}/\text{In}_y\text{Ga}_{1-y}\text{As}$ superlattices

R. Schwedler,* A. Ziebell, F. Brüggemann, B. Opitz, A. Kohl, and H. Kurz

Institut für Halbleitertechnik, Rheinisch-Westfälische Technische Hochschule Aachen, Sommerfeldstrasse 24, 52074 Aachen, Germany

(Received 2 May 1995)

We investigate strain-induced band-structure modifications of shallow $\text{In}_{1-x}\text{Ga}_x\text{As}/\text{In}_{1-y}\text{Ga}_y\text{As}$ ($x \approx 0.47$, $0.51 \leq y \leq 0.63$) Wannier-Stark superlattices grown by metal-organic vapor phase epitaxy. The strain-induced splitting between light-hole and heavy-hole bands is directly evidenced in photoluminescence experiments. The formation of minibands is investigated by photocurrent spectroscopy. With applied electric field, Wannier-Stark localization, Franz-Keldysh oscillations, and the quantum confined Stark effect are identified. Both type-I transitions between electrons and heavy holes and type-II transitions involving light holes are observed. We present a formalism to calculate the excitonic spectra of shallow strained superlattices. Excitonic binding energies are comparable to those found in InGaAs/InP quantum wells (type-I transitions) and bulk InGaAs (type-II transitions), respectively. The light-hole localization is shown to depend sensitively on both the strain and the superlattice layer thicknesses.

I. INTRODUCTION

Electro-optic modulators based on the Wannier-Stark effect (WSE) in semiconductor superlattices have found great interest in both basic and application-oriented research.¹⁻¹⁰ The WSE leads to significant modifications of the fundamental absorption in the presence of an electric field: (i) at the onset of the WSE, the absorption edge is blueshifted by about half the miniband (MB) width due to the localization of carrier wave functions^{1,2} and (ii) optical absorption spectra reveal a series of discrete, equally spaced steps in the WSE regime, with an energy splitting of the steps $\Delta E = eFd$, where F denotes the electric field in the layer direction and d is the period length. Recently, the time-domain equivalent of the WSE, Bloch oscillations, has also been detected.¹¹⁻¹³ The WSE appears to be interesting for electro-optic modulators⁴ and bistable devices.^{4,14-16} Particularly, high frequencies are expected when the concept of shallow superlattices is introduced.^{9,17,18}

Most experimental investigations on the WSE have been performed on $\text{AlGaAs}/\text{GaAs}$ superlattices (SL's).^{3-6,9,15,19,20} There is, however, great technological interest in InP -based material systems for the wavelength range between 1300 and 1550 nm. $\text{AlGaInAs}/\text{GaInAs}$,² InGaAs/InP ,^{21,22} and $\text{InGaAs}/\text{InAlAs}$ (Ref. 10) WSE modulators grown on InP have been reported. Little work has been done on WSE modulators grown by techniques other than molecular-beam epitaxy (MBE) and its variants. Growth of superlattice structures by metal-organic vapor phase epitaxy (MOVPE) appears particularly attractive for integration of modulator devices with laser emitters, which are routinely produced by MOVPE processes.

The major drawback of MOVPE growth is its apparent inability to produce short-period superlattices. This fail-

ure occurs (i) because of the incorporation of unwanted layers at the heterointerfaces during the gas switching sequences²³⁻²⁵ and (ii) because of the increased interface roughness with respect to MBE-grown material. For InP -based material systems, the interface layers are mainly formed by intermixing of the group-V compounds.²⁶⁻²⁸ They can be reduced by designing devices without any group-V gradient in the active region.²⁹

Our approach to WSE devices in the 1550-nm range is based on shallow $\text{In}_{1-x}\text{Ga}_x\text{As}/\text{In}_{1-y}\text{Ga}_y\text{As}$ superlattices,³⁰⁻³⁶ which do not exhibit any group-V gradients within the active layers. A peculiar feature to be expected for this class of materials is the mixed type-I/type-II valence band lineup. The highest valence-band maximum in tensile strained $\text{In}_{1-x}\text{Ga}_x\text{As}$ ($x > 0.47$) is formed by the light-hole valence band. For the light holes, the strain-induced splitting of the light-hole and heavy-hole valence bands tends to compensate the composition-induced change of the $\text{In}_{1-x}\text{Ga}_x\text{As}$ band gap.^{30,34,35} For $x > 0.47$, the light-hole band edge may be raised above the light-hole band edge of lattice-matched $\text{In}_{0.53}\text{Ga}_{0.47}\text{As}$. Therefore, in $\text{In}_{0.53}\text{Ga}_{0.47}\text{As}/\text{In}_{1-y}\text{Ga}_y\text{As}$ heterostructures, carrier-type-dependent confinement may occur, as illustrated in Fig. 1: The light holes are confined to the Ga-rich layers while electrons and heavy holes are confined to the lattice matched layers. This mixed type-I/type-II band structure implies, to a certain extent, separate tunability of the electron and light-hole MB's by variation of the appropriate layer widths and/or compositions.

There is, however, an ongoing debate about the band lineup proposed in Fig. 1 and its impact on the optical spectra. Magari *et al.*³³ and Okamoto *et al.*³⁴ have demonstrated polarization-insensitive tensile-strained $\text{In}_{0.53}\text{Ga}_{0.47}\text{As}/\text{In}_{1-y}\text{Ga}_y\text{As}$ waveguide amplifiers and lasers and interpreted the device performance by the strain-induced splitting of the valence bands. The band

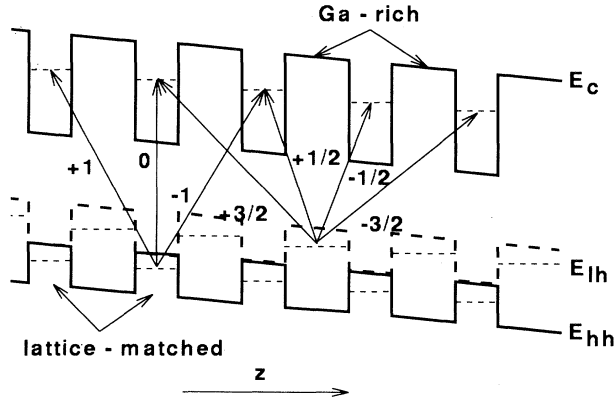


FIG. 1. Schematic representation of the band-edge profiles for a strained $\text{In}_{0.53}\text{Ga}_{0.47}\text{As}/\text{In}_{1-y}\text{Ga}_y\text{As}$ ($y > 0.47$) superlattice in the presence of an electric field. The solid (dashed) lines depict the conduction-band edge and the heavy-hole (light-hole) valence-band edge, respectively. The arrows indicate several possible type-I electron-heavy-hole ($n = 0, \pm 1$), and electron-light-hole transitions ($n = \pm 1/2, \pm 3/2$) resulting from the type-II band alignment.

structure proposed by them implies that the light holes are essentially unconfined.³⁴ A similar result was also obtained by Ishikawa and Bowers in their calculation of the $\text{In}_{1-x}\text{Ga}_x\text{As}/\text{InP}$ band lineup.³⁷ Zucker *et al.*³⁵ investigated comparable multiple-quantum-well samples by room-temperature photoluminescence spectroscopy. In marked contrast to Refs. 34 and 37, they argue that a small electron-light-hole overlap resulting from substantial type-II confinement is the reason for their failure to observe any light-hole-related features in the photoluminescence spectra.

The obvious discrepancy between these models of the $\text{In}_{0.53}\text{Ga}_{0.47}\text{As}/\text{In}_{1-y}\text{Ga}_y\text{As}$ band lineup can be clarified by experiments that are predominantly sensitive for the type-II configuration, such as analysis of the WSE: the type-I/type-II configuration manifests itself by the formation of two sets of Wannier-Stark ladders. The type-II ladders are unambiguously characterized by fractional Wannier-Stark indices ($\pm 1/2, \pm 3/2, \dots$) and by the lack of a field-independent transition.^{7,8}

We have recently reported growth and characterization of high-quality shallow $\text{In}_{0.53}\text{Ga}_{0.47}\text{As}/\text{In}_{1-y}\text{Ga}_y\text{As}$ multiple quantum wells,³⁸ by MOVPE and the observation of the WSE in $\text{In}_{0.53}\text{Ga}_{0.47}\text{As}/\text{In}_{1-y}\text{Ga}_y\text{As}$ superlattices.³⁹ In this work, we analyze in detail the band structure and the electro-optical properties of a set of $\text{In}_{1-x}\text{Ga}_x\text{As}/\text{In}_{1-y}\text{Ga}_y\text{As}$ ($x \approx 0.47, 0.54 \leq y \leq 0.61$) SL's with varying well and barrier widths by means of photocurrent (PC) and photoluminescence (PL) spectroscopy.

The paper is organized as follows. After a short description of the samples used for this work (Sec. II), we analyze the strain-induced splitting of light-hole and heavy-hole valence bands by temperature- and polarization-resolved PL. In Sec. IIIB, the WSE in

$\text{InGaAs}/\text{InGaAs}$ SL's is studied in PC experiments. In Sec. IV, we describe a model for the electronic states and optical transitions in shallow strained superlattices and compare it with our experimental observations. Our results are discussed and compared to previous results from the literature in Sec. V.

II. EXPERIMENT

The samples are grown by low-pressure MOVPE in a horizontal reactor with a total gas pressure of 20 hPa. The growth temperature is 604 °C. Trimethyl indium (TMI), trimethyl gallium (TMG), phosphine, and arsine (AsH_3) are used as precursors in H_2 carrier gas. The gas flow velocity is kept constant at 1.3 m/s. Two series of $\text{In}_{1-x}\text{Ga}_x\text{As}/\text{In}_{1-y}\text{Ga}_y\text{As}$ samples were grown for this work. Samples A and B are designed to investigate the band alignment of Ga-rich $\text{In}_{1-y}\text{Ga}_y\text{As}$ coherently strained to InP. After growth of a nominally undoped InP buffer layer on top of the n -InP (100) substrate, a 100-nm reference layer of $\text{In}_{0.53}\text{Ga}_{0.47}\text{As}$ is deposited and separated from the superlattice by 100-nm i -InP. The SL consists of 10 layers of nominally lattice-matched $\text{In}_{0.53}\text{Ga}_{0.47}\text{As}$ and 11 layers of Ga-rich $\text{In}_{1-y}\text{Ga}_y\text{As}$. The compositional changes within the SL are obtained by switching two TMI lines while the TMG and AsH_3 fluxes are kept constant. A growth interruption of 3 s under continuing AsH_3 flow is employed after each InGaAs layer to allow for smoothening of the interfaces. The samples are capped by 30 nm of undoped InP. The layer thicknesses and compositions are determined by x-ray diffractometry as described elsewhere.⁴⁰ They are summarized in Table I. For all samples, the total thickness of the strained layers is below the critical layer thickness.⁴¹⁻⁴⁴

The second series of samples (samples C, D, and E) is used for electro-optic characterization. In all cases, the SL consists of 10.5 periods. The SL is embedded in the intrinsic zone of a InGaAsP p - i - n diode. For this purpose, a n -InP buffer layer (100 nm) is grown on top of the n -InP substrate, followed by 100-nm lattice-matched n -InGaAsP [band gap E_g (2 K) ≈ 1 eV]. A nominally undoped 350-nm InGaAsP spacer layer is grown next. The SL consists of nominally lattice-matched wells and Ga-rich barriers. The barrier composition and layer thicknesses are varied as shown in Table I. The SL is topped by layers of i -InGaAsP (270 nm), p -InGaAsP (200 nm), and p^{++} - $\text{In}_{0.53}\text{Ga}_{0.47}\text{As}$ (30 nm) acting as a contact layer. The thickness of the depletion zone (L_d) differs from the total thickness of the nominally intrinsic zone (780 ± 10 nm for all p - i - n diodes investigated) due to diffusion of dopants during growth. We obtain $L_d = 750$ nm by CV etch profiling. Built-in voltages $U_{\text{BI}} = 0.35$ – 0.5 V ($T = 10$ K), depending on the sample, are estimated from a CV etch profile and from IV curves.

For PC spectroscopy, p - i - n diodes with ring-shaped Pd/Au Ohmic contacts (100 μm opening) are fabricated by liftoff. The contacts are not alloyed in order to avoid additional diffusion of dopants during this process. The top p^{++} - $\text{In}_{0.53}\text{Ga}_{0.47}\text{As}$ contact layer is selectively removed. Mesas (300 μm diameter) are defined by wet

TABLE I. Sample parameters determined from fitting x-ray data. Samples *A* and *B* are SL's embedded in undoped InP. In samples *C–E*, the SL is embedded in the intrinsic zone of an InGaAsP *p-i-n* diode. Also shown are the calculated confinement energies for electrons, light holes (LH's), and heavy holes (HH's). Note that the light holes are confined to the Ga-rich layers, whereas electrons and heavy holes are confined to the lattice-matched layers.

Sample	Barrier		Well		Confinement		
	$x_{\text{Ga},b}$	L_b (nm)	$x_{\text{Ga},w}$	L_z	Electrons (meV)	LH's (meV)	HH's (meV)
<i>A</i>	0.55	9.9	0.46	12.4	55	20	21
<i>B</i>	0.52	10.4	0.47	8.0	29	11	11
<i>C</i>	0.61	7.2	0.47	7.5	96	32	33
<i>D</i>	0.58	6.7	0.47	9.0	73	25	26
<i>E</i>	0.54	8.3	0.47	7.1	45	17	17

chemical etching. Substrate contact is made by silver glue.

PL and PC experiments are performed at temperatures between 10 K and 300 K. PL is excited by 5 mW of 632-nm HeNe laser radiation incident in the growth direction and observed either in the growth direction or in the direction of the quantum-well layers (edge emission). In the latter geometry, the emitted luminescence is led through a broadband polarizer for analysis of its polarization state. The luminescence is spectrally dispersed by a 0.5-m monochromator and detected with a Ge *p-i-n* diode cooled by liquid nitrogen. All PL spectra are corrected for the spectral sensitivity of the entire setup by means of a reference spectrum obtained from a calibrated tungsten lamp. The spectral resolution is better than 1 meV.

PC is excited by light from a 150-W tungsten lamp dispersed by a 0.25-m monochromator. The *p-i-n* diodes are biased using a computer-controlled low-noise reference voltage source. PC is recorded using a dc-picoamperemeter. Again, the spectral resolution is better than 1 meV.

III. RESULTS

A. Band lineup

PL spectroscopy is used to analyze the band lineup in the $\text{In}_{0.53}\text{Ga}_{0.47}\text{As}/\text{In}_{1-y}\text{Ga}_y\text{As}$ SL's *A* and *B*. The temperature-dependent PL emission in the growth direction of sample *A* is presented in Fig. 2. PL linewidths as low as 2.2 meV full width at half maximum at $T = 10$ K are observed. This linewidth is close to the theoretical lower limit of inhomogeneous line broadening of bulk $\text{In}_{0.47}\text{Ga}_{0.53}\text{As}$ imposed by alloy fluctuations.⁴⁵ We find no evidence for line broadening due to interface roughness or layer-width fluctuations.

The spectrum taken at $T = 10$ K exhibits two PL lines. The one at 803 meV is due to the reference layer of slightly In-rich ($x \approx 0.465$) $\text{In}_{1-x}\text{Ga}_x\text{As}$, while the higher-energy line at 811 meV is attributed to emission from the SL. On increase of the temperature, the low-energy peak decreases rapidly. This is characteristic for excitonic recombination from bulklike InGaAs layers.⁴⁶ At 70 K, the PL emission is substantially broadened due

to the thermal distribution of photogenerated carriers. An additional PL transition 17 meV above the PL peak energy is observed. With increasing temperature, the emission intensity from this transition increases with respect to the peak intensity. At room temperature, the high-energy line dominates the PL spectrum.

We further investigate the PL emission by analyzing its polarization state. Figure 3 shows typical room-temperature PL spectra of sample *B* emitted in the layer direction for TE and TM polarization, respectively. In addition to the main peak at 770 meV, both spectra show

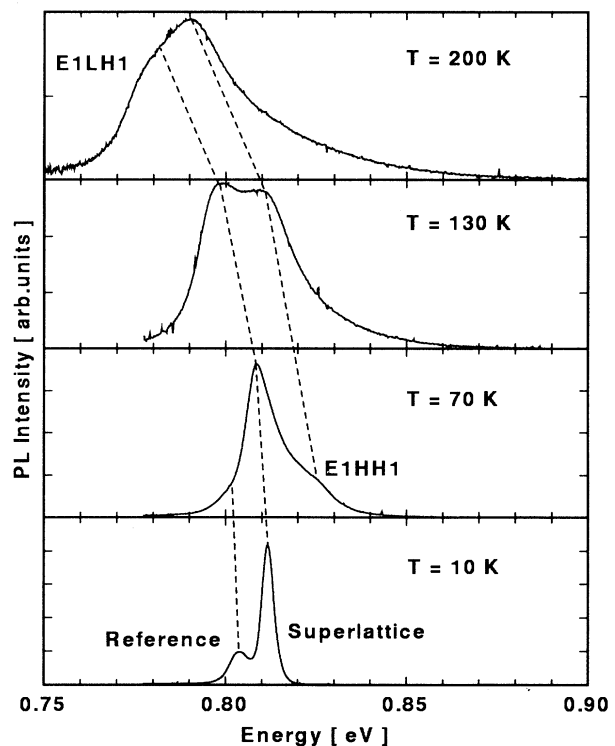


FIG. 2. PL spectra of sample *A* at various temperatures. The dashed lines are guides to the eye, visualizing the temperature dependence of the reference layer, electron–light-hole luminescence, and electron–heavy-hole luminescence, respectively.

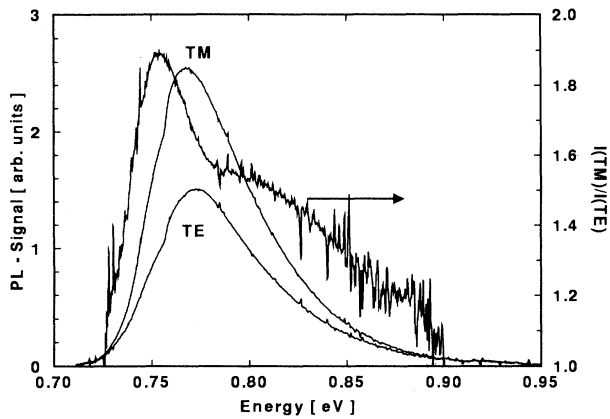


FIG. 3. Room temperature PL of sample *B* emitted in the direction of QW layers for TE and TM polarization. Also shown is the ratio of both spectra visualizing the strong energy dependence of the PL polarization.

a steplike feature at 756 meV. The intensity ratio of both spectra (Fig. 3) exhibits a maximum at 754 meV, which coincides with the position of the lower PL line read directly from the spectra.

Both temperature- and polarization-resolved PL spectra of Figs. 2 and 3 give evidence for the proposed band structure, with the uppermost valence band being attributed to light holes. This conclusion is based on two observations. (i) In the room-temperature PL spectra, a high-energy transition can dominate the PL only if the associated radiative transition matrix element is large compared to the matrix element of the lower transitions. Only for this case is the rapid decrease of carrier den-

sity at higher energies due to the Boltzmann distribution of photogenerated carriers compensated. As light-hole transitions are expected to be weaker than heavy-hole transitions, the lower-energy emission in Fig. 2 is likely to be associated with light holes. (ii) The polarized PL results confirm this model: the PL emission is expected to be essentially unpolarized for the electron-light-hole transition, but polarized in the TE mode for transitions involving heavy holes.⁴⁷ This agrees well with our observation of a lower TM to TE emission ratio at 770 meV with respect to 756 meV.

B. Type-I and type-II Wannier-Stark effect

The *p-i-n* diode samples *C-E* are characterized by PC spectroscopy at $T = 10$ K. We first discuss in detail the prototype PC spectra from sample *C* [Fig. 4(a)], followed by a description of the major differences in the spectra of the more shallow samples *D* and *E*. The spectra in Fig. 4(a) cover the bias range between 0.35 V and -3 V, corresponding to electric fields from flatband to 45 kV/cm. The strong absorption edge of the InGaAsP layers at 1 eV is not shown.

The spectrum at the highest forward bias ($U_b = +0.35$ V) exhibits two steps near 830 meV and 855 meV. The absence of any significant excitonic enhancement in the spectra indicates the MB regime in this bias range. As the bias changes towards $U_b = 0$ V, the relative intensity of the 855-meV signature increases and remains dominant for all reverse biases. At a bias around $U_b = 0$ V, excitonic enhancement of these two main structures indicates the onset of electron and light-hole wavefunction localization. With a further increase of the

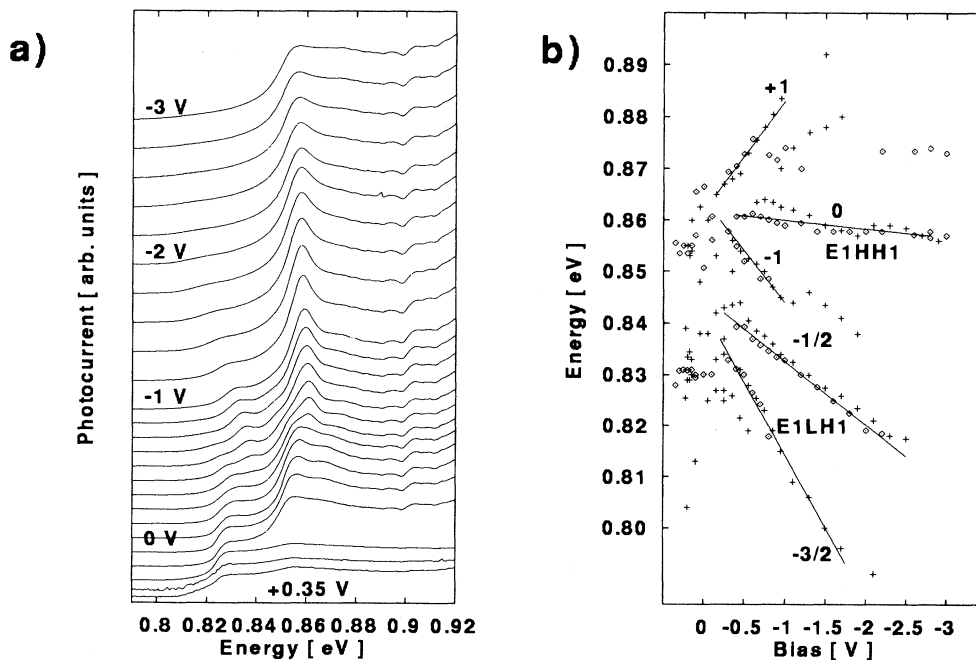


FIG. 4. (a) Low temperature PC spectra of the $\text{In}_{0.39}\text{Ga}_{0.61}\text{As}/\text{In}_{0.53}\text{Ga}_{0.47}\text{As}$ SL *C* taken at various bias voltages and (b) PC peak positions obtained directly from the spectra (\diamond) and after a derivation procedure ($+$). Solid lines are guides to the eye and are further explained in the text. The PC spectra at the highest forward biases ($U_b > 0.1$ V) have been rescaled for clarity.

reverse bias, the appearance of excitonic features and their field-induced splitting indicate the field localization regime. The bias dependence of the 830-meV transition and the 855-meV feature in this regime is very different. The step observed at 830 meV splits into two separate structures. Both structures strongly shift to lower energies, while their intensities rapidly decrease. They are observed for bias voltages up to -2 V. The 855-meV structure splits into a main line and several weak satellite features. The main line is blueshifted by 5 meV at bias around -0.5 V. The satellites originating from the 855-meV line vanish at bias voltages around -1 V.

The bias-dependent peak positions are plotted in Fig. 4(b). Several weak peaks are located by calculating the bias derivative of the spectra at bias voltages where the PC spectra themselves do not allow for precise determination of peak positions. The figure clearly shows the blueshift of the main spectral features around -0.2 to -0.4 V. Also, the 10-meV blueshift of the 830-meV absorption edge, which is hardly visible in the spectra due to multiple overlapping spectral features in this energy range, is clearly visible in Fig. 4(b).

Assuming that the blueshifts ΔE_b of each line originate from wave-function localization, they should be related to the zero-field MB widths ΔE and $\Delta_{\text{HH(LH)}}$ of electrons and heavy (light) holes, respectively, by $\Delta E_b = (\Delta_e + \Delta_{\text{HH(LH)}})/2 - \Delta E_{\text{HH(LH)}}^B$. Here $\Delta E_{\text{HH(LH)}}^B$ is the change in exciton binding energy for heavy- (light-) hole-related excitons by applying a bias. Taking into account the large effective mass of the heavy holes, the corresponding MB width Δ_{HH} is expected to be negligible compared to the MB widths of both electrons and light holes. This leads us to assign the strongly blueshifting 830-meV structure to the first electron MB to first light-hole MB transition (E1LH1), while the main absorption edge at 855 meV is attributed to the transition from the first electron MB to the first heavy-hole MB (E1HH1).

In the energy-voltage chart in Fig. 4(b), a linear shift of four peaks with increasing reverse biases is evident for $U_b < -0.5$ V. The main absorption edge, at 860 meV, exhibits only a very weak redshift even at the highest reverse biases. This particular behavior is attributed to the quantum-confined stark effect (QCSE) of a transition between electrons and heavy holes confined to the same layer. In terms of Wannier-Stark ladders, this is the spatially direct E1HH1(0) transition. The linear slopes in the energy-voltage chart in Fig. 4(b) for reverse bias $U_b < -0.3$ V indicate the formation of WSL's originating from oblique transitions between electrons and holes in adjacent confining layers. The slopes of the lines drawn in Fig. 4(b) are, within $\pm 10\%$, multiples of $ed\Delta F/\Delta U_b = 21$ meV/V, as indicated in the figure. They agree well with the change in the electric field estimated from the applied bias and the measured thickness of the intrinsic zone (19.6 mV/period per $\Delta U_b = 1$ V bias change).

For the Wannier-Stark ladders originating from the E1HH1 edge at 855 meV, the slopes are integer multiples of $ed\Delta F/\Delta U_b$, as expected for the WSE in type-I SL's. In contrast, the two lines originating from the E1LH1 MB clearly exhibit two different slopes corresponding

to fractions of the calculated field per SL period. The fractions are found to be $-1/2$ and $-3/2$, respectively. No corresponding positively indexed $+1/2, +3/2$ ladders are observed. These ladders would overlap with the main absorption edge and are therefore harder to detect than the background-free $-1/2$ and $-3/2$ ladders. In the Wannier-Stark regime, no bias-independent light-hole-related spectral structure is observed. It can be deduced from Fig. 1 that such a behavior is expected for transitions between electrons confined to the lattice-matched layer and light holes confined in the Ga-rich layer: The possible spatial separations d_n between a localized electron and the light-hole wave functions are given by $d_n = \pm(n + 1/2)d$ ($n = 0, 1, 2, \dots$). For this reason, only odd multiples of $ed\Delta F/(2\Delta U_b)$ are expected for the slopes of Stark ladder transitions in a type-II superlattice. Our measurements therefore directly prove the mixed type-I/type-II nature of the superlattice band structure.

C. Variation of the confinement potential

We compare the results from sample *C* to those from the more shallow samples *D* and *E*, with barrier Ga mole fractions of 0.58 and 0.54, respectively. The PC spectra and transition energies from sample *D* are shown in Fig. 5. Compared to sample *C*, the main E1HH1 MB absorption edge is redshifted by 25 meV due to both the smaller barrier band gap and the larger well width (see Table I). No strong absorption edge comparable to the E1LH1 MB absorption in sample *C* is observed at biases near flatband. This is a consequence of the reduction of confinement energy in the more shallow SL of sample *D*: the E1LH1 MB transition is expected to be very close to the strong E1HH1 MB absorption edge, which therefore partially masks the light-hole-related transition. Several series of field-dependent peaks are observed as the reverse bias is increased to -1.0 V. Two WSL's with linear slopes of -19 and 20 meV/V, respectively, are attributed to type-I E1HH1(± 1) transitions. No clear evidence for a light-hole-related WSL is found. Only a weak 825-meV spectral feature observed at reverse biases may be due to the E1LH1($-1/2$) transition. This assignment implies an anticrossing of heavy-hole- and light-hole-related states in the 825-meV range around zero bias, which may explain the lack of light-hole-related features in the forward bias regime.

Two blueshifting absorption structures are observed in the energy range between 840 meV and 880 meV. These transitions correspond to electronic states close to the SL barrier, where confinement occurs mainly due to the InGaAsP outer barriers above and below the SL. These states therefore form a quasicontinuum. The energy-voltage characteristics of the high-energy structures does not resemble those expected for either the WSE (linear) or the QCSE (quadratic decrease). We attribute them to Franz-Keldysh oscillations (FKO's), which are characterized by sublinear ($\Delta E_{\text{FKO}} \propto F^{2/3}$) field-induced shifts.⁴⁸ The solid lines in Fig. 5(b) are fits according to this relation.

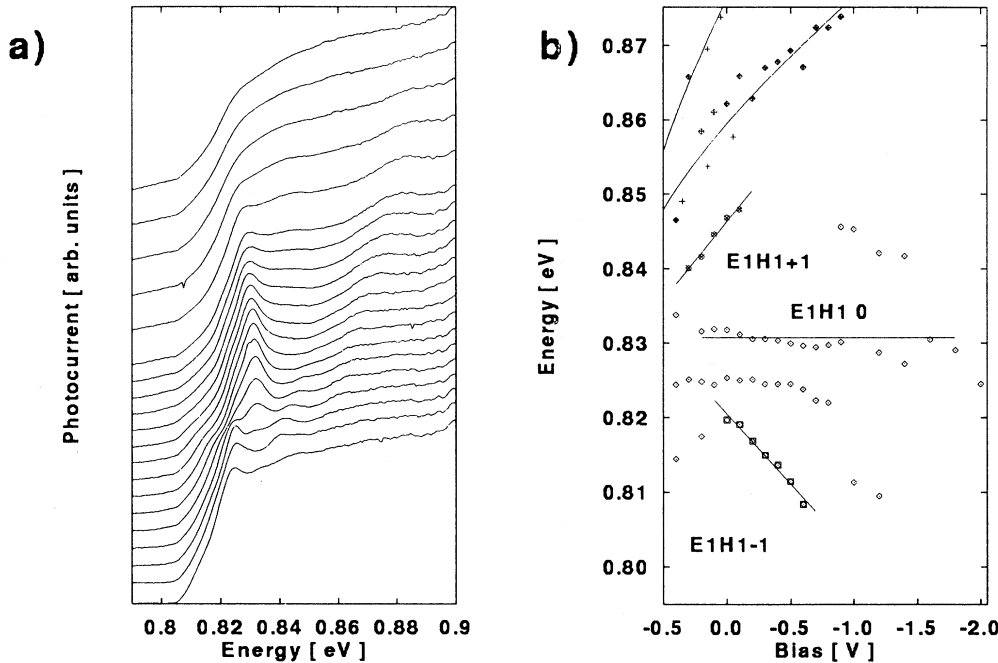


FIG. 5. (a) PC spectra taken at 10 K from sample *D* for various bias voltages and (b) PC peak positions for various bias voltages. The solid lines are guides to the eye, indicating (i) the Wannier-Stark transitions from superlattice confined states and (ii) the Franz-Keldysh oscillations observed in the superlattice continuum.

Sample *E* is the most shallow SL investigated in this study ($x_b = 0.54$). The well thickness is similar to that of sample *C* ($L_z = 7.1$ nm), but the barrier thickness is larger than in samples *C* and *D*. Field-dependent low-temperature PC spectra and PC peak positions from sample *E* are displayed in Fig. 6. In addition to the $E1HH1(\pm 1)$ Wannier-Stark ladders, the $E1LH1(-3/2)$ ladder, but no $E1LH1(-1/2)$ light-hole ladder, is ob-

served. The expected spectral position of the latter transition is close to the $E1HH1(-1)$ transition for a large bias range and may therefore be obscured by the stronger heavy-hole absorption. The $E1LH1$ MB absorption edge at 818 meV is well resolved in the forward-bias range. Compared to sample *D*, the smaller strain-induced valence-band splitting appears to be overcompensated by quantum-size effects due to the larger barrier

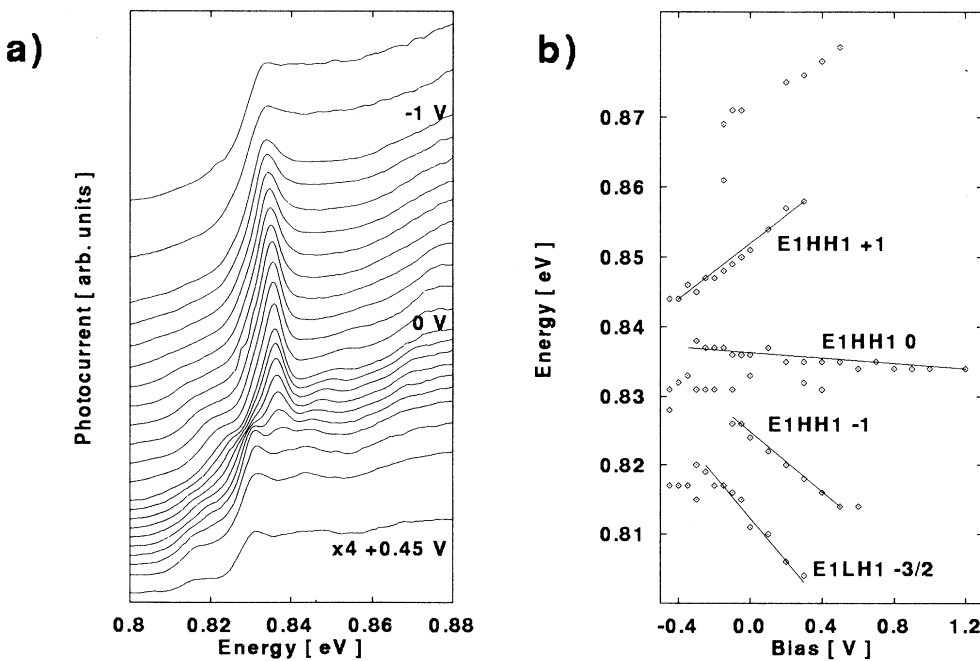


FIG. 6. (a) PC spectra ($T = 10$ K) and (b) PC peak positions from sample *E* for various bias voltages. The solid lines indicate various Wannier-Stark transitions.

width. Therefore, these measurements illustrate the separate tunability of heavy- and light-hole states in mixed type-I/type-II SL's.

IV. MODEL CALCULATION

In this section, we describe calculations of the electronic states and optical absorption spectra of shallow strained $\text{In}_{0.53}\text{Ga}_{0.47}\text{As}/\text{In}_{1-x}\text{Ga}_x\text{As}$ SL's. The calculated absorption spectra are then compared to our experimental data. To allow for comparison with differing results reported in the literature,^{34,49,41,50} we document in detail the interpolation of material parameters and band lineups used in this work.

A. Band lineup

Band gaps and band offsets of the strained InGaAs layers are determined from the material parameters of the binaries InAs and GaAs and of lattice-matched $\text{In}_{0.53}\text{Ga}_{0.47}\text{As}$ summarized in Table II. We use effective masses interpolated from those tabulated by Foulon *et al.*⁵¹ for $\text{In}_{1-x}\text{Ga}_x\text{As}$ on InP.

The band lineup of strained $\text{In}_{1-x}\text{Ga}_x\text{As}$ is calculated in two steps. First, the band gap $E_g(x)$ and the band offsets $E_v(x)$ and $E_c(x)$ for the valence band and the

conduction band of *unstrained* $\text{In}_{1-x}\text{Ga}_x\text{As}$ material are interpolated from the binary values. The band offsets within the InGaAs/InGaAs SL's are calculated from the band offsets of $\text{In}_{1-x}\text{Ga}_x\text{As}$ to InP, i.e., their associativity is assumed.

In a second step, strain contributions to the band edge energies are taken into account using the strain tensor components $e_{xx}(x) = [a_0(\text{InP}) - a(x)]/a_0(\text{InP})$ and $e_{zz}(x) = -[2C_{12}(x)/C_{11}(x)]e_{xx}(x)$, where $a(x)$ denotes the lattice constant of unstrained $\text{In}_{1-x}\text{Ga}_x\text{As}$ and $C_{ij}(x)$ are the components of the elastic stiffness tensor. The strain-induced changes in the band positions of conduction and valence bands due to the hydrostatic strain are obtained from $\Delta E_c(x) = a_c(x)[2e_{xx}(x) + e_{zz}(x)]$ and $\Delta E_v(x) = a_v(x)[2e_{xx}(x) + e_{zz}(x)]$, respectively. They depend on the hydrostatic pressure coefficients $a_c(x)$ and $a_v(x)$ for the conduction and valence band, respectively. Experimental data exist only for $a(x) = a_c(x) - a_v(x)$. We obtain the hydrostatic pressure coefficients given in Table II using the partitioning $|a_c(x)|/|a_v(x)| = 85:15$, which is consistent with recent calculations by Van de Walle for GaAs and InAs.⁵² Finally, the lack of valence-band degeneracy in the uniaxial strained material leads to the splitting of the light-hole ($\frac{3}{2} \pm \frac{1}{2}$) and heavy-hole ($\frac{3}{2} \pm \frac{3}{2}$) valence bands given by $\epsilon_0(x) = b_v(x)[e_{zz}(x) - e_{xx}(x)]$, where $b_v(x)$ is the valence-band shear strain coefficient.⁵³

The resulting band-edge energies of coherently strained

TABLE II. Material parameters used for calculations of band structure and optical transitions of the InGaAs/InGaAs superlattices. Material parameters for unstrained $\text{In}_{1-x}\text{Ga}_x\text{As}$ are linearly interpolated from the binary values, with the exceptions of lattice constants and band gaps, where quadratic interpolation including the lattice-matched ternary is used. Calculation of the material parameters of coherently strained $\text{In}_{1-x}\text{Ga}_x\text{As}$ is described in the text. The parameters for GaP are used to calculate the parameters of the InGaAsP barrier material by linear interpolation from the binaries.

	InP	GaAs	InAs	GaP	$\text{In}_{0.53}\text{Ga}_{0.47}\text{As}$	Unit
a_0 (4 K)	5.860 ^c	5.642 ^c	6.050 ^c	5.450 ^b	5.860 ^b	Å
E_g (4 K)	1.424 ^c	1.519 ^c	0.418 ^c	2.895 ^b	0.812 ^d	eV
Δ_0	0.11 ^c	0.34 ^c	0.37 ^c	0.08 ^b	0.355 ^c	eV
m_c^*	0.079 ^c	0.067 ^c	0.023 ^c	0.130 ^b	0.041 ^c	m_0
m_{LH}^*	0.121 ^c	0.094 ^c	0.027 ^c	0.17 ^b	0.056 ^c	m_0
m_{HH}^*	0.606 ^c	0.341 ^c	0.4 ^c	0.67 ^b	0.377 ^c	m_0
E_v	0	0.34 ^c	0.41 ^c	0.11 ^e	0.38 ^a	eV
C_{11}	10.22 ^f	12.11 ^c	8.541 ^c	14.39 ^b		10 ¹¹ dyn/cm ²
C_{12}	5.76 ^f	5.48 ^c	4.66 ^c	6.52 ^b		10 ¹¹ dyn/cm ²
b	-2.0 ^f	-1.7 ^f	-1.8 ^f	-1.5 ^f		eV
a	-6.6 ^g	-6.7 ^b	-6.0 ^g	-9.3 ^b		eV
a_v	0.99 ^h	1.005 ^h	0.9 ^h	1.395 ^h		eV
a_c	-5.61 ^h	-5.695 ^h	-5.1 ^h	-7.905 ^h		eV

^aInterpolated from the binary constituents.

^bReference 66.

^cReferences 67 and 68.

^dSlightly varying experimental values for the band gap of InGaAs lattice matched to InP are reported in the literature (Ref. 46).

^eEstimated after Ref. 69.

^fReference 70.

^gReference 71.

^hEstimated after Ref. 52 using a partitioning ratio $|a_c|/|a_v| = 85:15$.

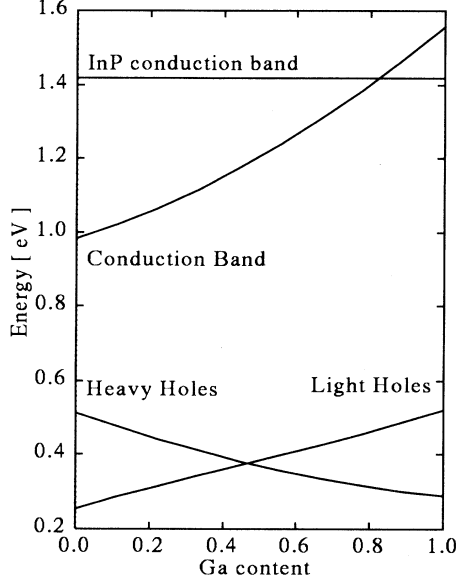


FIG. 7. Band edges of coherently strained $\text{In}_{1-x}\text{Ga}_x\text{As}$ depending on the composition calculated using the material parameters summarized in Table II. The energy scale is aligned to the InP valence-band edge.

$\text{In}_{1-x}\text{Ga}_x\text{As}$ on InP are summarized in Fig. 7, which also has been used to derive the schematic band lineup depicted in Fig. 1. The conduction band edge increases monotonically with Ga content of the strained layer. As mentioned above, the behavior of the valence-band edges is more complex due to the band splitting: the highest valence subband is formed by the heavy holes for compressively strained material ($x_{\text{Ga}} < 0.47$), but by the light holes for the tensile strained case. The light-hole and heavy-hole band offsets in $\text{In}_{1-x}\text{Ga}_x\text{As}/\text{In}_{1-y}\text{Ga}_y\text{As}$ SL's are found to be nearly equal, but opposite in sign, leading to the mixed type-I/type-II band alignment. The valence-band offsets in $\text{In}_{0.53}\text{Ga}_{0.47}\text{As}/\text{In}_{1-y}\text{Ga}_y\text{As}$ SL's turn out to be smaller than the conduction-band offset, making this material attractive for electro-optical modulator devices, where hole sweep-out times limit the device speed.⁵⁴

B. Electronic states and optical transitions

Based on the material parameters and on the band lineup, the electronic states are calculated by solving numerically the one-dimensional Schrödinger equation

$$\frac{\partial}{\partial z} \frac{1}{m_i(z)} \frac{\partial}{\partial z} \psi_{i,j}(z) + \frac{2}{\hbar^2} [E_{i,j} - V_i(z)] \psi_{i,j}(z) = 0 \quad (1)$$

for fields ranging from 0 to 35 kV/cm. Here the index i denotes electrons, heavy holes, or light holes and the potentials $V_i(z)$ account for both the spatial band-gap variations and for the electric field.

The numerical solution of Eq. (1) is performed for the complete SL (21 layers), limited by InGaAsP barriers,

as described above. For the numerical calculation, we use Numerov's algorithm, modified to take into account the effective-mass discontinuities.^{55,56} This algorithm is faster, and numerically more stable, than the usual approach using the transfer matrix method.⁵⁷ We note that we do not impose any *a priori* assumptions about the shape or localization of the wave functions. No special treatment for the spatially indirect electron-light-hole transitions is necessary.

Excitonic effects are treated in the framework of the model proposed by Leavitt and Little.^{58,59} The excitonic binding energy is calculated from

$$E_{ij}^B = \frac{\mu_{ij} e^4}{2\epsilon_r^2 \epsilon_0^2 \hbar^2} \int_{-\infty}^{\infty} dZ \int_{-\infty}^{\infty} dz |\psi_{e1,i}(z+Z)|^2 |\psi_{h,j}(z)|^2 \times w(Z \mu_{ij} e^2 / \epsilon_r \epsilon_0 \hbar^2), \quad (2)$$

where $w(z)$ is the excitonic binding energy for the simplified two-dimensional excitonic problem tabulated in Ref. 58 and μ_{ij} is the averaged optical density of states effective mass.⁵⁹

Based on the complete sets of transition energies, carrier wave functions, and exciton binding energies, excitonic absorption spectra for electron-light-hole and electron-heavy-hole transitions are calculated from a simplified version of Elliott's formula^{59,60}

$$\alpha(\hbar\omega) = \sum_{i,j} M_{ij}^2 \left[\frac{r}{\pi\delta} \exp\left(-\frac{(\hbar\omega - E_{ij} - E_{ij}^B)^2}{\delta^2}\right) + \frac{1}{2} \operatorname{erf}\left(\frac{\hbar\omega - E_{ij}}{\delta}\right) + \frac{1}{2} \right]. \quad (3)$$

Here M_{ij} are the single-particle wave-function overlap matrix elements, δ is a broadening parameter, and r allows us to adjust the relative strength of the discrete excitonic transitions with respect to the continuum. Throughout this work, we use $\delta = 8$ meV and $r = 25$ meV, which yield good agreement with experimental data. The PC signal is assumed to be proportional to the calculated absorption coefficient $\alpha(\hbar\omega)$; this assumption is justified provided (i) the total absorption is small and (ii) the photocurrent is saturated.⁶¹ For our samples, these conditions are met in all cases except for the spectra taken at the highest forward biases, where the SL's are not completely depleted.

C. Comparison to experimental results

We compare our experimental observations to results from the calculation of overlap matrix elements and excitonic absorption spectra. The field and spectral dependence of the single-particle wave-function overlap matrix elements M_{ij} calculated for sample C is depicted in Fig. 8, where energies of electron-heavy-hole [Fig. 8(a)] and electron-light-hole [Fig. 8(b)] transitions are plotted versus electric field. The widths of the markers indicate the magnitude of the corresponding electron-hole overlap integral, giving a measure of the oscillator strengths.

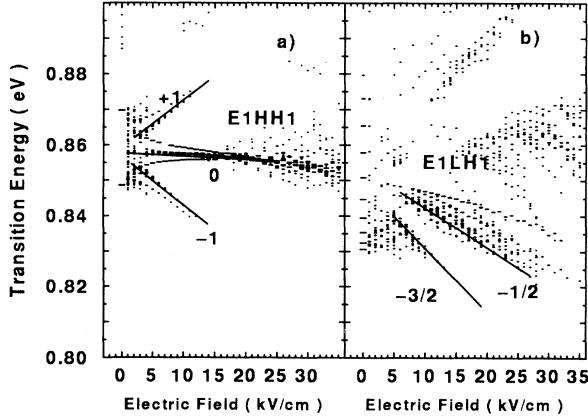


FIG. 8. Calculated transition energies ($T = 10$ K) for (a) electron-heavy-hole and (b) electron-light-hole transitions of sample *C*. Measured material parameters for sample *C* as given in Table I are used. The widths of the markers indicate the magnitude of the corresponding electron-hole overlap integral.

Because we calculate overlap matrix elements for all possible combinations of electron and hole wave functions, a great number of transitions is obtained.

Already at very low electric fields (1 kV/cm) the heavy holes are localized in the lattice-matched confining layers and a single-electron MB of 20 meV width is obtained. With increasing field, this broad miniband narrows due to the localization of the electron wave functions and forms the three Wannier-Stark transitions E1HH1(0) and E1HH1(± 1). However, the MB's do not collapse completely, as would be expected for an infinite SL. Due to the finite-size effect, side lobes corresponding to transitions occurring close to the limits of the SL appear in the vicinity of the main transitions.

For the electron-light-hole transitions [Fig. 8(b)], the low confinement energy and small effective mass of the light holes implies fully delocalized light holes (LH1) at zero field. As a matter of fact, the light-hole wave functions turn out to be even more spread out than those

of the electrons. The zero-field light-hole MB width almost equals the light-hole confinement. A very broad band (50 meV) of E1LH1 transitions is predicted. Above 5 kV/cm, the light holes localize partially and the formation of discrete transition bands indicates the formation of Wannier-Stark ladders. The type-II behavior of the light-hole transitions manifests itself through fractional Wannier-Stark indices in Fig. 8(b). The light-hole transition bands are rather broad. This broadening by 5–10 meV is caused by the large influence of the sample's boundaries on the transition energies of the weakly confined light holes. The broadening is strongest for the light-hole Wannier-Stark transitions with positive indices. This broadening due to the finite-size effect explains our failure to observe experimentally the E1LH1(+1/2) transition in any sample.

In Fig. 9, the calculated excitonic absorption spectra for samples *C* and *E* for electric fields of 0 kV/cm (MB regime), 10 kV/cm, and 15 kV/cm (WSE regime) are depicted. The spectra can be directly compared to the experimental ones in Figs. 4 and 6, taking into account a change of electric field of 13.3 kV/cm per 1 V bias change. The general shape of the simulated spectra of the absorption coefficient agrees well with the experimental PC spectra. For sample *C*, the theoretical transition energies agree with the experimental ones within a few meV. For sample *E*, however, the values deviate by as much as 10 meV. These deviations may arise from the determination of the layer parameters by x-ray diffractometry, where only the average SL composition and the SL period length are obtained with high precision. A reasonable error of $\Delta x_{\text{Ga}} = 1\%$ in the determination of the individual layer compositions, corresponding to an $\text{In}_{1-x}\text{Ga}_x\text{As}$ band-gap change of 10 meV, may explain the observed discrepancy.

The calculated excitonic binding energies of the E1HH1(0) transitions, of 6–10 meV at maximum, turn out to be similar to those observed in InGaAs/InP QW's.⁶² The binding energies of the E1LH(-1/2) excitons (3–5 meV) are found to be lower and similar to the binding energies of bulk InGaAs light-hole excitons⁶² due to the large spatial extension of the wave functions involved. Exciton binding energies of similar magnitude have been observed in $\text{In}_{1-x}\text{Ga}_x\text{As}/\text{GaAs}$ superlat-

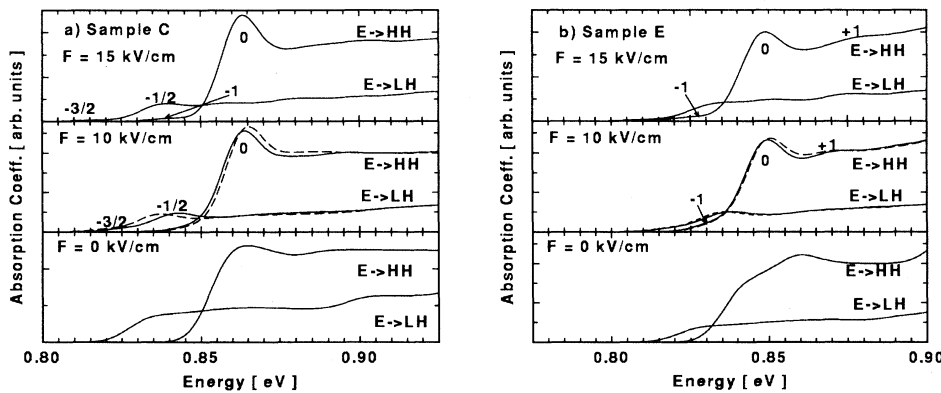


FIG. 9. Simulated absorption spectra for samples *C* and *D* and electric fields of 0 kV/cm (MB regime), 10 kV/cm, and 15 kV/cm (WSE regime). The dashed lines depict results from a calculation using a slightly different set of parameters, as described in the text.

tices with comparable, very small confinement energies.⁶³ This leads to a large excitonic enhancement of the E1HH1(0) transitions and to an almost undetectable excitonic enhancement of the E1LH1(-1/2) transition. All other Wannier-Stark transitions exhibit negligible exciton binding energies.

V. DISCUSSION

In this section, we summarize our results and compare them with the literature. We found that the lowest valence band in shallow tensile strained $\text{In}_{0.53}\text{Ga}_{0.47}\text{As}/\text{In}_{1-x}\text{Ga}_x\text{As}$ SL's is formed by the light holes. The Wannier-Stark effect is observed for both electron-light-hole and electron-heavy-hole transitions even in the most shallow $\text{In}_{0.53}\text{Ga}_{0.47}\text{As}/\text{In}_{0.46}\text{Ga}_{0.54}\text{As}$ sample. The observation of Wannier-Stark ladders with fractional indices unambiguously proves the type-II configuration of the light holes. Despite the type-II configuration, strong luminescence and absorption structures from the electron-light-hole transitions are observed.

These findings are in contrast to some common assumptions about type-II superlattices in general and about strained $\text{In}_{0.53}\text{Ga}_{0.47}\text{As}/\text{In}_{1-y}\text{Ga}_y\text{As}$ heterostructures in particular. Type-II transitions are commonly associated with small oscillator strengths due to small electron-hole overlap integrals, which limit their usefulness in device applications.^{47,35,64,65} This assumption is not applicable to shallow superlattices. As a matter of fact, our model calculations indicate, for a large range of electric fields, type-II overlap integrals larger than those calculated for the type-I electron-heavy-hole transitions. The overlap is determined by the wave-function localization rather than by the band alignment. The experimentally observed lower absorption strengths and room-temperature PL intensities of the light-hole transitions are solely determined by the different densities of states for both hole species. This result is in contradiction to the observations of Zucker *et al.*,³⁵ who explained their failure to observe light-hole related PL room-temperature emission from $\text{In}_{0.53}\text{Ga}_{0.47}\text{As}/\text{In}_{1-y}\text{Ga}_y\text{As}$ by the type-II alignment. The authors of Ref. 35, however, do not report any polarization-sensitive characterization, which could reveal light-hole-related signatures.

We do not claim verification of the complete band-structure parameter set (Table II) and of our interpolation procedure. Our results, however, impose strong restrictions on several band-structure parameters of $\text{In}_{0.53}\text{Ga}_{0.47}\text{As}/\text{In}_{1-y}\text{Ga}_y\text{As}$. The observation of type-II Wannier-Stark ladders directly proves that substantial confinement acts on the light holes even in very shallow $\text{In}_{0.53}\text{Ga}_{0.47}\text{As}/\text{In}_{1-y}\text{Ga}_y\text{As}$ SL's. The band-structure models of Okamoto *et al.*³⁴ and Ishikawa and Bowers,³⁷ which predict negligible valence-band offsets for the light holes, are clearly in disagreement with our experimental findings. Our calculations yield a valence-band alignment that is almost completely determined by the shear-strain-induced splitting between light-hole and heavy-hole band edges. The valence-band changes caused by composi-

tional variation and by hydrostatic strain nearly cancel each other. We checked this property of the band lineup by repeating our model calculations for a $|a_c|/|a_v|$ partitioning ratio of 2:1 instead of 85:15, 2:1 being the lowest value reported in literature.^{49,41,50} Results from this calculation are displayed in Fig. 9 (dashed lines). A similar effect on the proposed band lineup may also be obtained by using different values for the band offsets of unstrained $\text{In}_{1-x}\text{Ga}_x\text{As}$. The resulting light-hole-heavy-hole splitting is generally smaller by about 10 meV than that obtained with the original set of parameters and therefore leads to poor agreement between experimental and theoretical spectra.

Our analysis of $\text{In}_{0.53}\text{Ga}_{0.47}\text{As}/\text{In}_{1-y}\text{Ga}_y\text{As}$ modulator devices, as well as recent works on lasers³⁴ and light amplifiers,^{32,33} indicates that MOVPE-grown shallow strained SL's are suitable for electro-optical devices in the 1550-nm range. Such devices are particularly interesting where polarization-independent operation is required. However, the excitonic linewidth of such WSE devices still needs to be improved. We have demonstrated that the main reason of inhomogeneous line broadening in our SL's is the finite-size effect. We therefore expect that increasing the number of superlattice periods will lead to a decrease of linewidth. This, however, requires use of strain balanced heterostructures³¹ to increase the critical layer thickness.

VI. CONCLUSION

We have reported optical and electro-optical characterization of shallow tensile-strained $\text{In}_{0.53}\text{Ga}_{0.47}\text{As}/\text{In}_{1-y}\text{Ga}_y\text{As}$ Wannier-Stark effect superlattices. Due to strain splitting of the valence-band edges, the lowest band gap in this material system corresponds to electron-light-hole transitions. The type-II light-hole band alignment is directly deduced from photocurrent spectra for $0.54 \leq y \leq 0.61$. The unusual valence-band alignment of the light holes leads to Wannier-Stark transitions with fractional indices. Light-hole-related Wannier-Stark ladders are observed only if the splitting between light-hole- and heavy-hole-related transitions is sufficiently large and generally not observed for positive Wannier-Stark indices. Strong excitonic enhancement of the low-temperature electron-heavy-hole absorption edge is found, corresponding to exciton binding energies similar to those observed in $\text{In}_{0.53}\text{Ga}_{0.47}\text{As}/\text{InP}$ multiple quantum wells. In contrast, the electron-light-hole absorption edge exhibits negligible excitonic enhancement. A detailed model of the field-dependent excitonic absorption spectra agrees quantitatively with experimental photocurrent data. The large bias sensitivity of the fundamental absorption edges implies that $\text{In}_{1-x}\text{Ga}_x\text{As}/\text{In}_{1-y}\text{Ga}_y\text{As}$ and related superlattice materials are attractive for the realization by MOVPE of highly effective modulator devices in the 1550-nm range.

ACKNOWLEDGMENTS

We like to thank S. Juillaguet, J. Camassel, and G. C. Cho for useful discussion about the band structure of $\text{In}_{1-x}\text{Ga}_x\text{As}/\text{In}_{1-y}\text{Ga}_y\text{As}$, and F. Royo and B.

Fraisse for x-ray characterization. We thank Y. Dhaibi for many discussions about the numerical treatment of superlattice confined states, and H. G. Roskos and K. Wolter for critical reading of the manuscript. This work was supported by the Deutsche Forschungsgemeinschaft under Contract No. Ku540/11-3.

- * Present address: GES-CNRS, cc074 UM2 "Sciences et Techniques," Place Eugène Bataillon, 34095 Montpellier cedex 5, France.
- ¹ J. Bleuse, G. Bastard, and P. Voisin, *Phys. Rev. Lett.* **60**, 220 (1988).
 - ² J. Bleuse, P. Voisin, M. Allovon, and M. Quilicq, *Appl. Phys. Lett.* **53**, 2632 (1988).
 - ³ P. Voisin *et al.*, *Phys. Rev. Lett.* **61**, 1639 (1988).
 - ⁴ I. Bar-Joseph *et al.*, *Appl. Phys. Lett.* **55**, 340 (1989).
 - ⁵ F. Agulló-Rueda, E. E. Mendez, and J. M. Hong, *Phys. Rev. B* **40**, 1357 (1989).
 - ⁶ E. E. Mendez, F. Agulló-Rueda, and J. M. Hong, *Appl. Phys. Lett.* **56**, 2545 (1990).
 - ⁷ M. K. Saker *et al.*, *Phys. Rev. B* **43**, 4945 (1991).
 - ⁸ M. K. Saker *et al.*, *Superlatt. Microstruct.* **10**, 295 (1991).
 - ⁹ K. W. Goossen, J. E. Cunningham, and W. Y. Jan, *Appl. Phys. Lett.* **59**, 3622 (1991).
 - ¹⁰ E. Bigan *et al.*, *Appl. Phys. Lett.* **60**, 1936 (1992).
 - ¹¹ J. Feldmann *et al.*, *Phys. Rev. B* **46**, 7252 (1992).
 - ¹² K. Leo *et al.*, *Solid State Commun.* **84**, 943 (1992).
 - ¹³ C. Waschke *et al.*, *Phys. Rev. Lett.* **70**, 3319 (1993).
 - ¹⁴ K. Law, R. Yan, J. Merz, and L. Coldren, *Appl. Phys. Lett.* **56**, 1886 (1990).
 - ¹⁵ G. R. Olbright, T. E. Zipperian, J. Klem, and G. R. Hadley, *J. Opt. Soc. Am. B* **8**, 346 (1991).
 - ¹⁶ M. Hosada, K. Kawashima, K. Tominaga, and K. Fujiwara, *Solid State Electron.* **37**, 847 (1994).
 - ¹⁷ J. Feldmann *et al.*, *Appl. Phys. Lett.* **59**, 66 (1991).
 - ¹⁸ G. von Plessen *et al.*, *Appl. Phys. Lett.* **63**, 2372 (1993).
 - ¹⁹ E. E. Mendez, F. Agulló-Rueda, and J. M. Hong, *Phys. Rev. Lett.* **60**, 2426 (1988).
 - ²⁰ H. Schneider, A. Fischer, and K. Ploog, *Phys. Rev. B* **45**, 6329 (1992).
 - ²¹ C. W. Chen *et al.*, *J. Appl. Phys.* **74**, 5895 (1993).
 - ²² C. Rigo *et al.*, *Mater. Sci. Eng. B* **28**, 305 (1994).
 - ²³ T. Y. Wang, E. H. Reihlen, H. R. Jen, and G. B. Stringfellow, *J. Appl. Phys.* **66**, 5376 (1989).
 - ²⁴ R. Schwedler *et al.*, *Mater. Sci. Eng. B* **20**, 66 (1993).
 - ²⁵ W. Seifert, D. Hessman, X. Liu, and L. Samuelson, *J. Appl. Phys.* **75**, 1501 (1994).
 - ²⁶ S. Juillaguet *et al.*, in *Non-Stoichiometry in Semiconductors*, edited by K. J. Bachmann, H.-L. Hwang, and C. Schwab (North-Holland, Amsterdam, 1992), pp. 155–160.
 - ²⁷ R. Schwedler *et al.*, *Appl. Surf. Sci.* **63**, 187 (1993).
 - ²⁸ J. P. Wittgreffe, M. J. Yates, S. D. Perrin, and P. C. Spurdens, *J. Cryst. Growth* **130**, 51 (1993).
 - ²⁹ A. Mircea, A. Ougazzaden, G. Primot, and C. Kazmierski, *J. Cryst. Growth* **124**, 737 (1992).
 - ³⁰ G. C. Osbourn, *Phys. Rev. B* **27**, 5126 (1983).
 - ³¹ M. Quilicq *et al.*, *J. Appl. Phys.* **59**, 2447 (1986).
 - ³² K. Magari *et al.*, *IEEE Phot. Technol. Lett.* **2**, 556 (1990).
 - ³³ K. Magari, M. Okamoto, and Y. Noguchi, *IEEE Phot. Technol. Lett.* **3**, 998 (1991).
 - ³⁴ M. Okamoto *et al.*, *IEEE J. Quantum Electron.* **27**, 1463 (1991).
 - ³⁵ J. E. Zucker, C. H. Joyner, and A. G. Dentai, *IEEE Phot. Technol. Lett.* **4**, 432 (1992).
 - ³⁶ A. Godefroy *et al.*, in *Proceedings of the International Conference on InP and Related Materials* (Société des Electriciens et des Electroniciens, Paris, 1993), pp. 143–146.
 - ³⁷ T. Ishikawa and J. E. Bowers, *IEEE J. Quantum Electron.* **50**, 562 (1994).
 - ³⁸ A. Kohl *et al.*, *Mater. Sci. Eng. B* **21**, 244 (1993).
 - ³⁹ R. Schwedler *et al.*, *Appl. Phys. A* **57**, 199 (1993).
 - ⁴⁰ F. Royo *et al.*, *Superlatt. Microstruct.* **15**, 187 (1994).
 - ⁴¹ T. Y. Wang and G. B. Stringfellow, *J. Appl. Phys.* **67**, 344 (1990).
 - ⁴² R. People and J. C. Bean, *Appl. Phys. Lett.* **47**, 322 (1985).
 - ⁴³ R. People and J. C. Bean, *Appl. Phys. Lett.* **49**, 229 (1986).
 - ⁴⁴ J. W. Matthews and A. E. Blakeslee, *J. Cryst. Growth* **25**, 118 (1974).
 - ⁴⁵ M. Engel *et al.*, *J. Cryst. Growth* **93**, 359 (1988).
 - ⁴⁶ K.-H. Goetz *et al.*, *J. Appl. Phys.* **54**, 4543 (1983).
 - ⁴⁷ G. Bastard, *Wave Mechanics Applied to Semiconductor Heterostructures* (Éditions de Physique, Les Ulis, 1988).
 - ⁴⁸ C. K. Inoki *et al.*, *Phys. Rev. B* **49**, 2246 (1994).
 - ⁴⁹ S. L. Chuang, *Phys. Rev. B* **43**, 9649 (1991).
 - ⁵⁰ M. Sugawara, N. Okazaki, T. Fujii, and S. Yamazaki, *Phys. Rev. B* **48**, 8102 (1993).
 - ⁵¹ Y. Foulon, C. Priester, G. Allan, and M. Lannoo, in *Proceedings of the 20th International Conference on the Physics of Semiconductors*, edited by E. M. Anastasakis and J. D. Joannopoulos (World Scientific, Singapore, 1990), Vol. 2, pp. 977–980.
 - ⁵² C. G. Van de Walle, *Phys. Rev. B* **39**, 1871 (1989).
 - ⁵³ Band mixing leads to an additional but negligible correction of the light-hole valence-band edge.
 - ⁵⁴ A. M. Fox *et al.*, *IEEE J. Quantum Electron.* **27**, 2281 (1991).
 - ⁵⁵ J. P. Killingbeck, *Microcomputer Quantum Mechanics* (Hilger, Bristol, 1983).
 - ⁵⁶ P. Leisching *et al.*, *Phys. Rev. B* **50**, 14389 (1994).
 - ⁵⁷ A. K. Ghatik, K. Thyagarajan, and M. R. Shenoy, *IEEE J. Quantum Electron.* **24**, 1524 (1988).
 - ⁵⁸ R. P. Leavitt and J. W. Little, *Phys. Rev. B* **42**, 11774 (1990).
 - ⁵⁹ R. P. Leavitt and J. W. Little, *Phys. Rev. B* **42**, 11784 (1990).
 - ⁶⁰ R. J. Elliott, *Phys. Rev.* **108**, 1384 (1957).
 - ⁶¹ R. P. Leavitt, J. L. Bredshaw, J. T. Pham, and M. S. Tobin, *J. Appl. Phys.* **75**, 2215 (1994).
 - ⁶² M. Grundmann and D. Bimberg, *Phys. Rev. B* **38**, 13486

- (1988).
- ⁶³ B. Soucail *et al.*, *Phys. Rev. B* **41**, 8568 (1990).
- ⁶⁴ S. Li and J. B. Khurgin, *Appl. Phys. Lett.* **61**, 1694 (1992).
- ⁶⁵ J. Böhrer, A. Krost, and D. Bimberg, *J. Vac. Sci. Technol. B* **11**, 1642 (1993).
- ⁶⁶ *Zahlenwerte und Funktionen aus Naturwissenschaft und Technik*, edited by O. Madelung, M. Schulz, and H. Weiss, Landolt-Börnstein, New Series, Group III, Vol. 17, Pt. a (Springer-Verlag, Berlin, 1982).
- ⁶⁷ D. Gershoni, H. Temkin, M. B. Panish, and R. A. Hamm, *Phys. Rev. B* **39**, 5531 (1989).
- ⁶⁸ D. Gershoni, H. Temkin, and M. B. Panish, *Phys. Rev. B* **38**, 7870 (1988).
- ⁶⁹ W. A. Harrison and J. Tersoff, *J. Vac. Sci. Technol. B* **4**, 1068 (1986).
- ⁷⁰ S. Adashi, *J. Appl. Phys.* **53**, 8775 (1982).
- ⁷¹ E. P. O'Reilly, *Semicond. Sci. Technol.* **4**, 121 (1989).